Desalination and Water Treatment 319 (2024) 100407

Contents lists available at ScienceDirect

Desalination and Water Treatment

journal homepage: www.sciencedirect.com/journal/desalination-and-water-treatment/

Porous sodium alginate/poly (acrylic acid) composites cross-linked with $FeCl_3$ for acid black 1 dye removal from aqueous solution

Endar Hidayat[a,b,c,*], Nur Maisarah Mohamad Sarbani[a,b], Sadaki Samitsu[c], Yoshiharu Mitoma[d], Mitsuru Aoyagi[a,b], Seiichiro Yonemura[a,b], Hiroyuki Harada[a,b]

[a] Graduate School of Comprehensive Scientific Research, Prefectural University of Hiroshima, Shobara 727-0023, Japan
[b] Department of Life System Science, Faculty of Bioresources Science, Prefectural University of Hiroshima, Shobara 727-0023, Japan
[c] Data-driven Polymer Design Group, Research Center for Macromolecules and Biomaterials, National Institute for Materials Science, 1–2-1 Sengen, Tsukuba 305-0047, Japan
[d] Department of Integrated Science and Engineering for Sustainable Societies, Faculty of Science and Engineering, Chuo University, Tokyo 112-8551, Japan

ARTICLE INFO

Keywords:
Sodium alginate
Poly (acrylic acid)
Acid black 1 removal
Adsorption
Wastewater treatment

ABSTRACT

This study developed a polymeric composite, sodium alginate (SA)/poly (acrylic acid) (PAA) cross-linked with $FeCl_3$ (SA/PAA-Fe), for its function as adsorbent to eliminate acid black 1 dye (AB1) from an aqueous solution. The structural analysis of SA/PAA-Fe revealed a porous structure. To comprehensively evaluate the adsorption of AB1 onto SA/PAA-Fe and gain insight into its mechanism, we examined the effects of solution's pH, initial dye concentration, adsorbent dosage, contact time, and adsorption temperature. The best adsorption conditions for achieving a highly effective removal percentage of 95.43 % were a pH of 8.9, contact period of 90 min, and a temperature of 45 °C. Pseudo-second-order and Langmuir models were fitted for the isotherm and kinetic model parameters, respectively. Thermodynamic analyses strongly suggested that the adsorption process occurred was endothermic and spontaneous. The adsorption of AB1 was primarily observed on the solid surface, as confirmed by the SEM-EDS and FTIR measurements.

1. Introduction

The continued expansion of the industrial sectors inevitably lead to various environmental problems, due to the usage of enormous amounts of chemicals [1]. In particular, the availability of safe water is one of the most serious global challenges owing to the limited access to freshwater. Rivers are important sources of drinking water and also help to maintain diverse aquatic ecosystems that provide food sources for humans and animals. Rivers are an important component of earth's landforms and carry nutrients to the oceans by flowing water from sedimentary areas. However, they have been considered as sites for dumping undesirable materials and chemicals by careless people and businesses. The primary threat to water security is the unmitigated release of pollutants of diverse origins directly into aquatic ecosystems without sufficient treatment [2,3]. Organic dyes, which are commonly used for color clothing, are pollutants that need to be treated for environmental protection. In particular, azo dyes, identified by the presence of azo (-N = N-) groups, are toxic, carcinogenic, and mutagenic to organisms. Acid black 1 dye (AB1) is one of the organic dyes which is extensively utilized in cosmetic items, and can poses risk to cause irritation to the skin, and respiratory system as well as may potentially trigger severe and chronic toxicity [4].

Several traditional chemical, physical, and biological techniques have been shown to effectively eliminate azo dye pollutants. However, concerns persist regarding their operational expenses, removal efficacy, and the potential creation of secondary pollutants [5]. Amongst all the efficient removal method, adsorption has emerged as a successful strategy for removing azo dyes from water. This method is not only economically viable, but also boasts a remarkable retention efficiency while avoiding the generation of secondary pollution [2,6,7]. In this regard, different types of materials have been explored as potential adsorbent which are classified into two types: porous and non-porous. Examples of non-porous adsorbents include barium sulfate and graphite soot [8] whereas porous adsorbents such as metal-organic frameworks (MOF) [9], polymer-coated MCM-41 [10], and ZR-BDC-CP [11] have been utilized for the adsorption of synthetic dyes. However, better adsorbent qualities, such as fast adsorption and superior mechanical strength for repeated use, are still required.

* Corresponding author at: Graduate School of Comprehensive Scientific Research, Prefectural University of Hiroshima, Shobara 727-0023, Japan.
E-mail address: hidayatendar1@gmail.com (E. Hidayat).

https://doi.org/10.1016/j.dwt.2024.100407
Received 7 May 2024; Received in revised form 20 May 2024; Accepted 20 May 2024

Versatile functional material such as poly (acrylic acid) (PAA) offers a promising approach for developing functional materials that can be used for pollution removal. This was attributed to the carboxyl (COOH) groups present in each monomer unit of PAA, which significantly enhanced the number of active surface sites. PAA is a polymer derived from acrylic acid that exhibits robust adhesion and recyclability, while also possessing non-toxic characteristics. Unfortunately, the conversion of PAA to hydrogel has encountered some issues, including a lack of mechanical strength and susceptibility to damage during fabrication and repeated usage in water [12]. The strength of the resultant material is an important aspect that need to be considered to ensure effective application. Certain materials such as polysaccharide possess the capacity to mitigate mechanical aging due to their structural composition, which includes several functional groups that can enhance mechanical strength. Thereby, addition of this material may provide mechanical strength for PAA. Study by Chen et al. [13] concluded that mechanical performance of PAA is significantly enhanced by the interaction with cellulose.

Sodium alginate (SA) is a polysaccharide polymer with linear structure extracted from brown algae, which a naturally occurring polyelectrolyte salt [14–16]. This polymer is comprised of α-l-guluronic (G) and β-d-mannuronic (M) acid residues, forming a continuous 1,4-bond that differs from that of other substances. SA contains a significant presence of functional groups, such as hydroxyl (OH) and COOH groups, in addition to negatively charged sites. Such functionalized groups play a crucial role in the capture of molecular pollutants in water. SA is often used to transform soft weak hydrogels into stiff strong gel beads by introducing ionic crosslinking assisted by divalent cations such as Ca^{2+}. This method has been frequently used for the elimination of heavy metals [17] and methylene blue [18,19]. SA hydrogel may have certain limitation in its mechanical strength [20]. However, previous study has successfully produced a hydrogel from a combination of PAA/alginate with high percentage (96 %) removal for methylene blue dye [21]. Based on this information, the utilisation of material through the combination of SA and PAA could potentially serve as an efficient approach to tackle environmental pollution. Unlike previous studies, this current work aims to transform the polymer mixture into a microparticle instead of hydrogel, as a consideration to address the concern related to the limitation of hydrogel's mechanical.

Currently, there is a growing interest in trivalent-cross-linked alginate, an alginate-based hydrogel beads crosslinked with trivalent cations such as Fe^{3+}, because of its ability to enhance the mechanical stability, porosity, and absorptivity of gels compared to other ionotropic alginates [22]. Meanwhile, alginate-based microparticles have attracted much attention due to their unique pore structures, long-term stability that allow for the effective azo dyes adsorption. Polymer microparticles are often used in the pharmaceutical [23], food, and cosmetic [24] sectors. However, not much research has been done on the adsorptive removal of azo dyes from water. Therefore, it was crucial to evaluate its effectiveness.

In this study, SA-PAA composite particles with interpenetrated networks crosslinked with trivalent crosslinking of Fe^{3+} (SA/PAA-Fe) were synthesized. The polymer composite particles were then employed as adsorbents for the removal of AB1 dye from aqueous solution. The characteristics of the particles were assessed using SEM-EDS, XRD, FTIR, N_2 gas adsorption, and pH_{zpc}. The adsorption process was comprehensively analyzed using adsorption isotherms, kinetics, and thermodynamics.

2. Materials and methods

2.1. Materials

Kanto Chemical Co. Inc., Japan, supplied Acid Black 1 (AB1), Ferric Chloride ($FeCl_3$), hydrochloric acid (HCl) and sodium hydroxide (NaOH). Sodium alginate was purchased from Wako Chemical Industries (Osaka, Japan). Poly (acrylic acid) (MW: 100,000) was purchased from Scientific Polymer Products, INC, New York.

2.2. Preparation of SA/PAA-Fe

The SA/PAA-Fe adsorbents were synthesized using the following procedure. A mixture containing 6 mL of aqueous SA solution with 1 wt % concentration, 6 mL of aqueous PAA solution (5 wt%), 1 mL of 3 M NaOH solution, and 1 mL of distilled water was prepared in a bottle flask. The mixture was then stirred with a magnetic stirrer for one hour at room temperature. The mixture was introduced dropwise into a 10 wt% aqueous $FeCl_3$ solution using a syringe. After 90 min, the SA/PAA-Fe was then washed using ethanol and distilled water and then dried at 60 ˚C for 24 h. The collected adsorbent was pulverized using a mortar and sieved to ≤ 425 μm for further experiments.

2.3. Batch adsorption experiments

In a series of experiments, the effects of several factors, including initial pH, AB1 solution concentration, adsorbent dosage, adsorption duration, and temperature, on the removal of AB1 were investigated. Batch adsorption tests were conducted by immersing the SA/PAA-Fe in 50 mL of AB1. A UV-Vis spectrophotometer (JASCO V-530) was used to identify the concentration of AB1 that remained after the experiment at a wavelength of 621 nm. The following equations are used to determine the removal percentage (*Removal* (%)) and adsorption equilibrium amount (q_e (mg/g)).

$$\text{Removal}(\%) = \frac{C_i - C_e}{C_i} \times 100 \quad (1)$$

$$q_e\,(\text{mg/g}) = \frac{C_i - C_e}{W} \times V \quad (2)$$

Where *Removal (%)* is the removal efficiency and C_i and C_e are the initial and equilibrium AB1 concentrations (mg/L), respectively. where q_e is the equilibrium adsorption capacity of the adsorbent (mg/g), W is the amount of adsorbent (g), and V is the volume of AB1 solution (L).

2.4. Analytical measurements

Nitrogen adsorption/desorption experiments was performed at 77 K using a gas adsorption analyzer (BELSORP-max, MicrotracBEL, Japan). The surface areas of SA/PAA-Fe were calculated from the nitrogen adsorption isotherm based on the Brunauer-Emmett-Teller (BET) model. The crystalline configuration of the SA/PAA/Fe was analyzed using powder X-ray diffraction (XRD) with Cr/Kα radiation (λ = 2.2909 Å, MiniFlex, Rigaku, Japan). Fourier-transform infrared spectroscopy (FTIR) spectra were obtained using a Thermo Scientific Nicolet iS10 instrument (Thermo Fisher Scientific Inc., Waltham, MA, USA) both before and after AB1 adsorption. The structural surface of the SA/PAA-Fe composite was observed by scanning electron microscopy-energy dispersive X-ray spectroscopy (SEM-EDS) (Miniscope TM4000PlusII, Hitachi-hitech, Tokyo, Japan). The neutral surface charge, or pH_{zpc} value, was computed using the following formula: pH_{zpc} = pH-final − pH-initial.

3. Results and discussion

3.1. Characterization of SA/PAA-Fe

Fig. 1a. displays the N_2 adsorption/desorption isotherms and Table 1 summarizes the Brunauer-Emmett-Teller (BET) specific surface area (S_{BET}), total pore volume (V_{total}), and pore size (D_{meso}) of the adsorbent. The adsorbent exhibited a mesoporous structure with a size of 19.1 nm, as defined by [25]. However, it possessed only a small specific surface area and total pore volume of 1.6 $m^2\ g^{-1}$ and 0.008 $cm^3\ g^{-1}$,

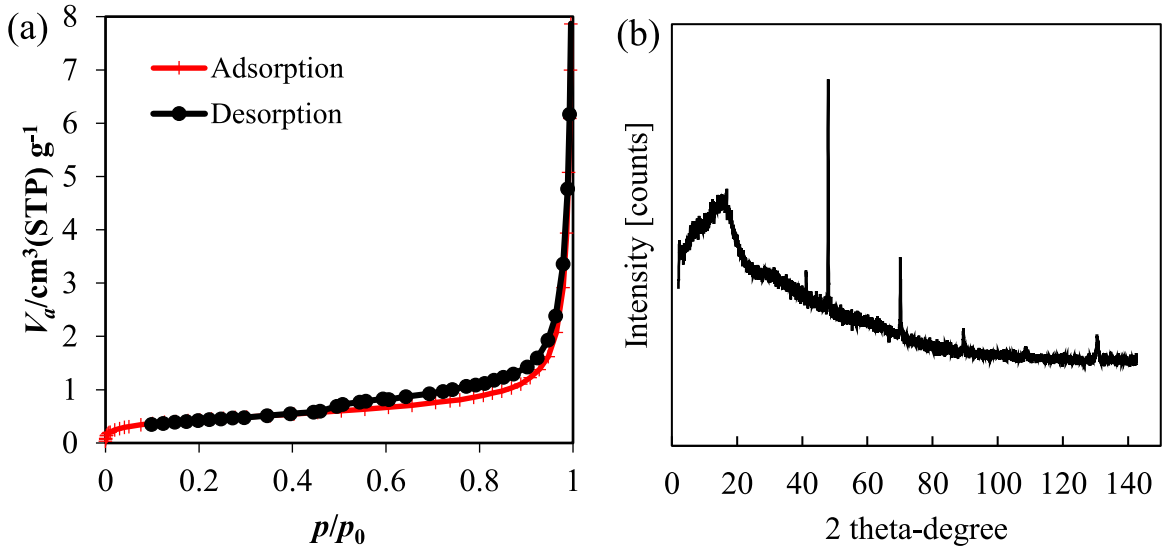

Fig. 1. (a) N_2 adsorption/desorption of SA/PAA-Fe (b) XRD spectra of SA/PAA-Fe.

respectively. X-ray diffraction (XRD) spectra of the SA/PAA-Fe adsorbent is shown in Fig. 1b. The XRD peaks at 2θ = 7.00° and 16.01° suggest that SA/PAA-Fe was amorphous, which might be explained by the major components of SA and PAA. Moreover, the diffraction peaks seen at 2θ = 41.16°, 47.91°, 70.08°, 89.35°, 108.60°, and 130.34° may be attributed to Halite (JCPDS 01–076-3452), which may be slightly contaminated on the collection process of SA/PAA-Fe.

The morphology of SA/PAA-Fe before and after AB1 adsorption was obtained by using scanning electron microscopy (SEM) is presented in Fig. 2. The picture shows that the surface of the adsorbent was rough before adsorption, and became flat and smooth after AB1 adsorption. Table 2 presents the weight percentage (wt%) of the element from EDS data. The analysis revealed that the synthesized SA/PAA-Fe compound consisted of carbon (C), oxygen (O), iron (Fe), chloride (Cl), and sodium (Na). Moreover, the detection of sulfur (S) and nitrogen (N) components after AB1 adsorption suggests that AB1 molecules were captured at the surface of the SA/PAA-Fe adsorbent.

The FT-IR spectra of the adsorbent and the AB1-loaded adsorbent are shown in Fig. 3. The peak decrease after AB1 adsorption from 3170 cm^{-1} to 2936 cm^{-1} is expected to be due to the functional groups that engage in the process of adsorption through the interactions of intermolecular bonds, such as van der Waals and (-OH) bonding interactions [26]. The peak at 1701 cm^{-1} was assigned to C═O [27]. A decrease in the peak intensity was detected at 1570 cm^{-1} to 1541 cm^{-1}, which was assigned to the stretching of –COO$^-$ [27,28]. The peak at 1172 cm^{-1} represents the C-O bond. A shifted peak occurred from 656 cm^{-1} to 648 cm^{-1} and 604 cm^{-1} to 599 cm^{-1}, corresponding to Fe-O. While most of the peaks were consistent after adsorption, some were shifted to lower wavenumbers, indicating the influence of stronger intermolecular interactions between SA/PAA-Fe and the AB1 dye. According to the IR analysis, both electrostatic attraction and intermolecular interactions connecting the functional compositions of SA/PAA-Fe and AB1 dye molecules likely contribute to dye adsorption. The possible mechanism of AB1 adsorption onto SA/PAA-Fe is illustrated in Fig. 4.

Table 1
Characteristics of SA/PAA-Fe.

Adsorbent	S_{BET} [m^2 g^{-1}]	V_{total} [cm^3 g^{-1}]	D_{meso} [nm]
SA/PAA-Fe	1.6	0.008	19.1

3.2. Initial pH effect and surface charge of adsorbent (pH_{zpc})

The pH of the adsorption system influences the ionization of the adsorbates and surface charge of the adsorbent material [29]. Fig. 5a. shows the adsorption of AB1 when the pH of the AB1 solution was changed. The percentage of removal decreased and then increased within this pH range (2.7 to 10). A pH of 8.9 was optimal for adsorption, resulted in a removal percentage of 97.7 %. Fig. 5b. shows that the adsorbent exhibited a negative surface charge, whereas AB1 had a positive charge under alkaline conditions. This finding demonstrates that the electrostatic connection of the SA/PAA-Fe and AB1 dyes has a greater impact than the pH of the solution.

3.3. Effect of initial concentration

The adsorption removal of AB1 on SA/PAA-Fe was studied by varying the initial AB1 concentration in the range of 10 to 50 mg/L. The adsorption experiment was performed under a contact period of 30 min, pH of 8.9, adsorbent amount of 0.05 g/50 mL, and temperature of 25 °C. Increasing the AB1 concentration to 50 mg/L reduced the AB1 removal percentage on the SA/PAA-Fe surface (Fig. 6). The adsorbed amount of AB1 was calculated to be 10–21 mg/L, which is almost independent of the initial concentration of AB1. This is because of the presence of excess AB1 molecules, which are much larger than the number of available sites of SA/PAA-Fe for adsorption.

3.4. Effect of adsorbent dosage

To assess the impact of the quantity of adsorbent used in the adsorption of AB1, several quantities of SA/PAA-Fe were introduced, ranging from 0.05 to 0.5 g, in a 50 mL solution. The research were conducted using an initial AB1 concentration of 50 mg/L adjusted to pH 8.9 at 25 °C. Fig. 7 shows the effects of adsorbent quantity on AB1 adsorption. Increasing the adsorbent dosage can increased the removal percentage from 24.0 % to 77.8 % (Fig. 7a). This could be ascribed to the increase in the SA/PAA–Fe active sites, leading to an enhanced removal percentage due to the adsorption-desorption equilibrium. In contrast, the adsorption capacity of SA/PAA–Fe decreased (12.00 to 3.89 mg/g), as the adsorbent dosage increase (Fig. 7b). This is because of the reduced availability of active adsorbent sites caused by the accumulation and overlapping of the adsorbent particles [30]. This study

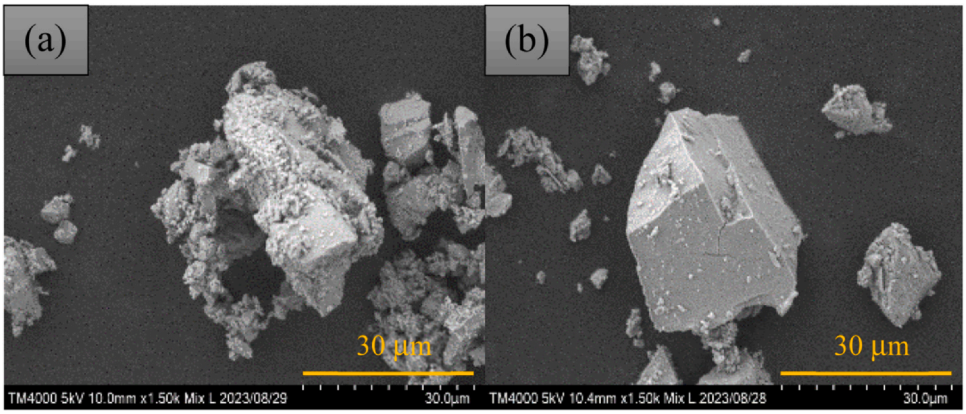

Fig. 2. SEM images (a) before and (b) after the adsorption of AB1.

Table 2
EDS data of SA/PAA-Fe before and after adsorption.

Parameters (wt%)	Before adsorption	After adsorption
C	48.94	49.54
O	19.95	18.62
Fe	21.27	28.85
Cl	8.97	0.68
Na	0.87	0.15
S		0.12
N		2.05

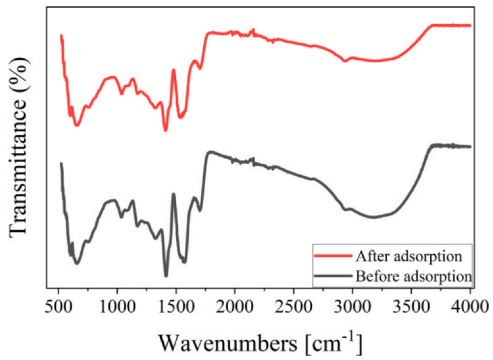

Fig. 3. FTIR spectra of SA/PAA-Fe before and after AB1 adsorption.

matches the findings of [31], in which a zeolite/chitosan hydrogel was used to remove Acid Red 88.

3.5. Adsorption isotherm analysis

The adsorption isotherms were analysed by applying the Langmuir in Eq. (3) and Freundlich in Eq. (5) models to the adsorption experimental data. Table 3 depicts the value of the linear regression coefficient (R^2) obtained from Fig. 8, in conjunction with the additional adsorption isotherm characteristics. The Langmuir model fits the AB1 dye adsorption data better than the Freundlich model, as evidenced by the higher R^2 values. The R_L and *1/n* values are < 1. Therefore, the adsorption process using this indicator was verified to be favorable. These findings suggest that adsorption process occurred in a monolayer condition at the adsorption sites on the surface of SA/PAA-Fe.

$$C_e/q_e = \left(\frac{C_e}{q_{max}}\right) + 1/(K_L q_{max}) \quad (3)$$

$$R_L = \left(\frac{1}{1 + bC_o}\right) \quad (4)$$

$$\ln q_e = \ln K_F + \frac{1}{n} \ln C_e \quad (5)$$

where q (mg/g) is the adsorption capacity, C_e (mg/L) is the equilibrium concentration, q_{max} (mg/g) is the maximum adsorption capacity, C_0

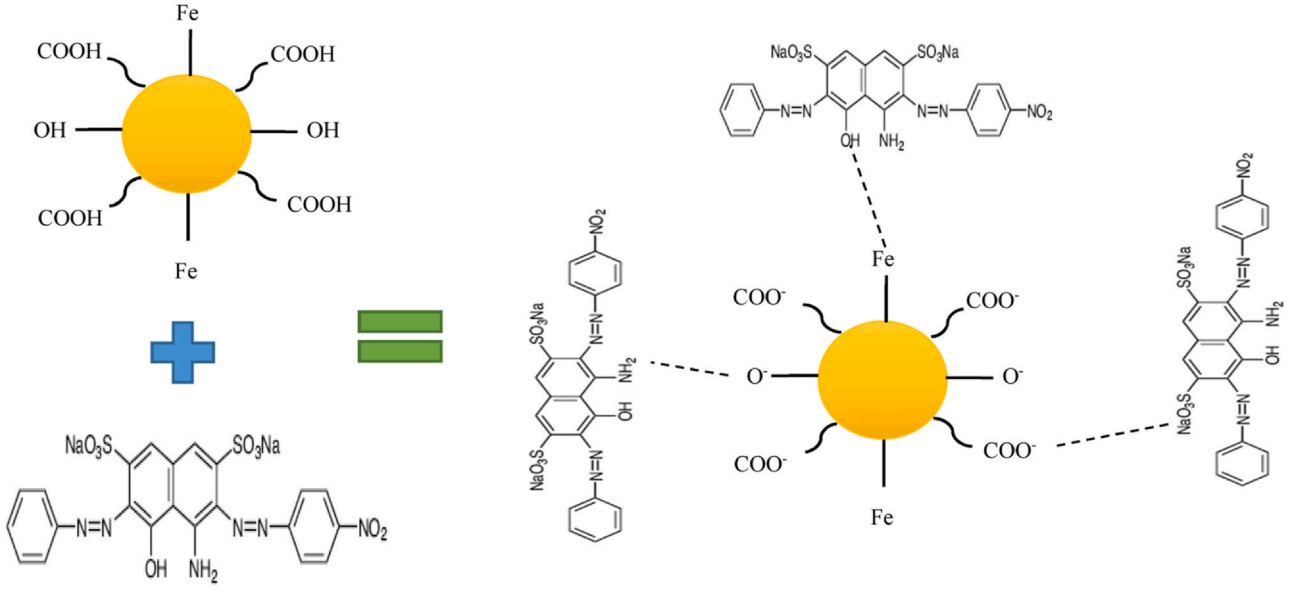

Fig. 4. Proposed AB1 adsorption mechanisms.

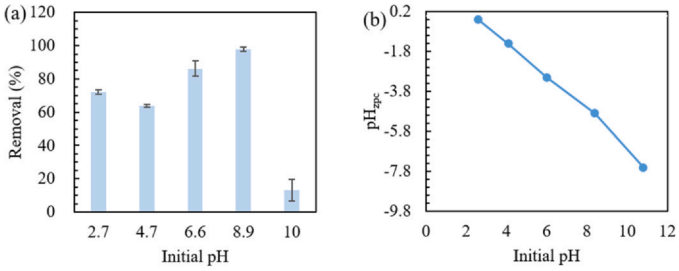

Fig. 5. (a) Initial pH effect versus removal percentage (b) Surface charge (pH_{zpc}) of SA/PAA-Fe.

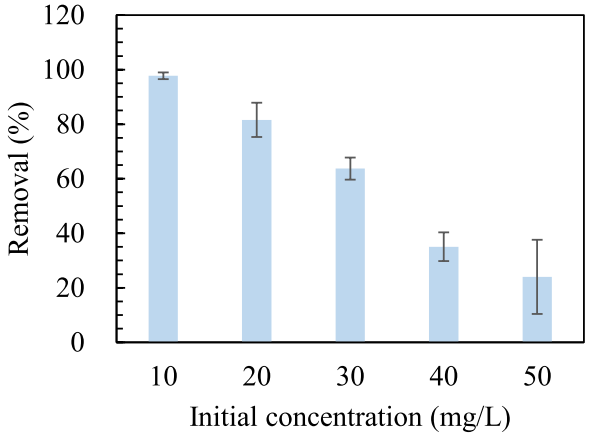

Fig. 6. Effect of the initial AB1 dye concentration on the removal percentage.

(mg/L) is the initial concentration, R_L is a greater coefficient indicating a stronger adsorption capacity, $R_L > 1$ (unfavorable), $R_L = 1$ (linear), and $0 < R_L$ (favorable). K_L (L/mg) and K_F (mg/g) are the equilibrium constants of adsorption and $1/n$ is the adsorption intensity.

3.6. Effect of contact time and kinetic experiment studies

The effect of adsorption times (30–90 min) on the adsorption of AB1 using SA/PAA-Fe at a dye concentration of 50 mg/L and adsorbent concentration of 0.5 g/50 mL of adsorbent is shown in Fig. 9. The original pH was maintained and the adsorption data are shown in Fig. 5. Observations indicate that the removal percentage declined between 30 and 45 min but then significantly increased at 60 min. It eventually reached equilibrium after 90 min, with 84.1 % dye removal and an adsorption capacity of 4.20 mg/g.

The results from kinetic models provided valuable insights into the adsorption process. The data obtained from the AB1 adsorption on the

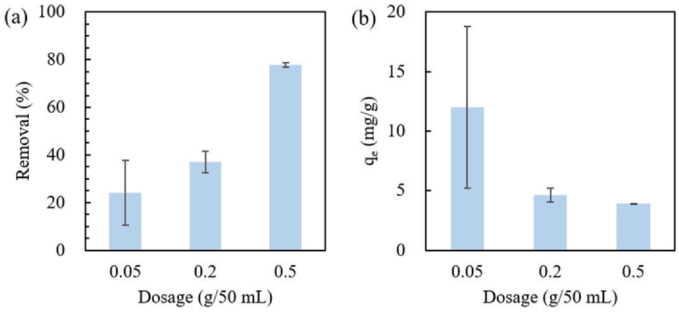

Fig. 7. Effect of adsorbent dosage on (a) removal percentage and (b) adsorption capacity of AB1.

Table 3
Isotherm model for adsorption AB1 onto SA/PAA-Fe.

Isotherm models	Parameters	Value
Langmuir	q_{max} (mg/g)	12.0952
	K_L (L/mg)	7.3905
	R^2	0.9841
	R_L	0.0014
Freundlich	K_F (g/mg $min^{-1})^n$	331.8751
	1/n	0.0597
	R^2	0.2210

SA/PAA-Fe surface were evaluated using two kinetic models: the pseudo-first-order model in Eq. (6) and pseudo-second order in Eq. (7).

$$\log(q_e - q_t) = \log q_e - k_1 t \quad (6)$$

$$t/q_t = 1/(k_2 q_e^2) + t/q_e \quad (7)$$

where k_1 (min^{-1}) is the rate constant of the pseudo-first-order model and t (min) is the time. Linear plots of log t against log (q_e-q_t) and t against t/q_t were used to determine k_1 and k_2 from the slope of the linear plots of the pseudo-first-order and pseudo-second-order models, respectively.

The kinetic variables and linear correlation coefficients for AB1 adsorption are displayed in Fig. 10, and Table 4. The R^2 value of the pseudo-second-order kinetic model (R^2 = 0.9971) was much higher compared to the pseudo-first-order kinetic model (R^2 = 0.0116), indicating that the process of adsorption is controlled by chemisorption. The findings were related with previous works conducted by [32–34], who utilize CS/ZL/ZrO/Fe_3O_4 for phosphate adsorption, coffee husk biochar-Fe_3O_4 for glyphosate adsorption and carboxylmethyl cellulose-chitosan magnetite for Cr (VI) and Pb (II) adsorption, respectively.

3.7. Adsorption thermodynamic study

In the adsorption of AB1, the impact of certain variables, such as temperature has been investigated at temperatures of 298, 308, and 318 K. Fig. 11, demonstrates that higher temperatures can enhance the removal percentage and adsorption capacity from 84.08 to 95.43 % and 4.20 to 4.77 mg/g, respectively. This increased, may be due to the enhanced interaction between SA and PAA, leading to the formation of more active adsorption sites at high temperatures, resulting in an increase in the adsorption amount.

The following Gibbs` and Van`t Hoff equations were used to visually derive the thermodynamic parameters (ΔG^o, ΔH^o and ΔS^o):

$$\Delta G^\circ = -RT \ln K \quad (8)$$

$$\Delta G^\circ = \Delta H^\circ - T\Delta S^\circ \quad (9)$$

$$\ln K = \frac{\Delta S^\circ}{R} - \frac{\Delta H^\circ}{RT} \quad (10)$$

Where K is the equilibrium constant, R (J.mol $^{-1}$ K $^{-1}$) is the gas constant, T (K) is the temperature, ΔG° is the Gibbs free energy (kJ mol $^{-1}$), ΔS° is the entropy (kJ mol $^{-1}$), and ΔH° is the enthalpy (kJ mol $^{-1}$). ΔH° and ΔS° were obtained from the slope and intercept of the plot of ln$K$ versus $1/T$.

The effect of temperature on the adsorption of AB1 on the Van`t Hoff diagram is illustrated in Fig. 12. Table 5 presents a list of plot parameters. The Gibbs free energy (ΔG°) value at 308 and 318 K are negative, which corresponds with the thermodynamic constants shown in Table 5 and is consistent with the ΔS°value ($\Delta S > 0$ = spontaneous process). The positive ΔH° values indicate an endothermic adsorption process [35]. This endothermic condition in the adsorption process has

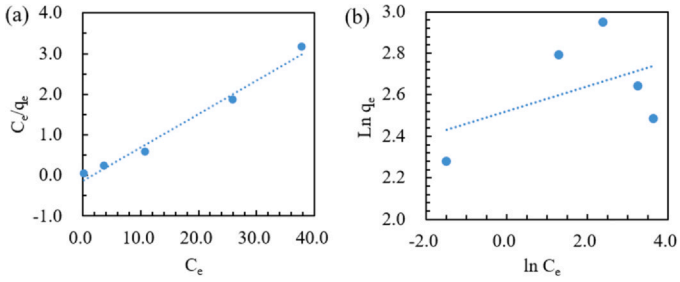

Fig. 8. Adsorption isotherms of AB1 analyzed by (a) Langmuir (b) Freundlich models.

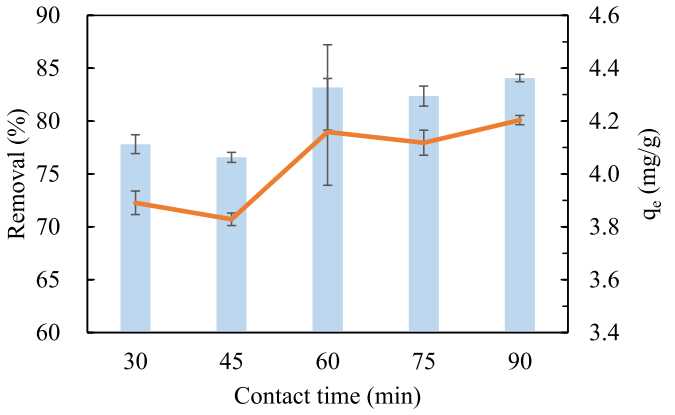

Fig. 9. Removal percentage and adsorption capacity of AB1 vs. contact time (min).

Table 4
Kinetic model parameters for adsorption AB1 onto SA/PAA-Fe.

Kinetic models	Parameters	Value
Pseudo-first-order	q_e (mg/g)	2.2628
	K_1 (min^{-1})	0.00004
	R^2	0.0116
Pseudo-second-order	q_e (mg/g)	4.4307
	K_2 (g/mg min^{-1})	0.04391
	R^2	0.9971

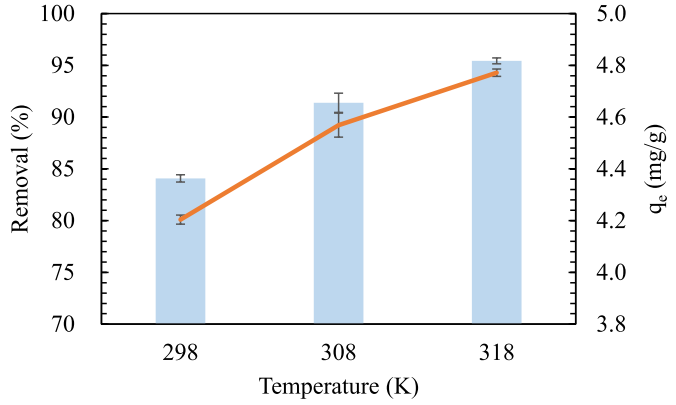

Fig. 11. Effect of temperature on AB1 adsorption onto SA/PAA-Fe.

also been demonstrated in several previous studies on the adsorption of RB5 dye onto powdered banana peel [36] and heavy metal adsorption onto FCPNC [37].

3.8. Regeneration of AB1 adsorption

An analysis on adsorbent's regeneration is important for understanding the efficiency of the adsorbent in repeatedly adsorbing AB1 molecules. During the regeneration analysis of SA/PAA-Fe, a solution containing acetone and deionized water was used to eliminate the AB1 from the adsorbent. Fig. 13 demonstrated the hydrogel's ability to be reused for a maximum of five cycles. The data indicate that SA/PAA-Fe consistently demonstrated a reduction in its adsorption capacity.

3.9. Comparison SA/PAA-Fe and other adsorbents

Table 6 presents a comparison of adsorption capacity for an anionic dyes as reported in similar studies. These capacities vary significantly due to differences in sample pre-treatment, pH levels, dosage amounts, contact times, and temperatures. A critical distinction is the particle size of the SA/PAA-Fe. The limited surface area measured at 1.6 m^2/g resulted in fewer active sites available for adsorption, which led to a reduced capacity. Nonetheless, the adsorption capacity of SA/PAA-Fe falls within a moderately intermediate range, making it a feasible option for the removal of anionic dyes.

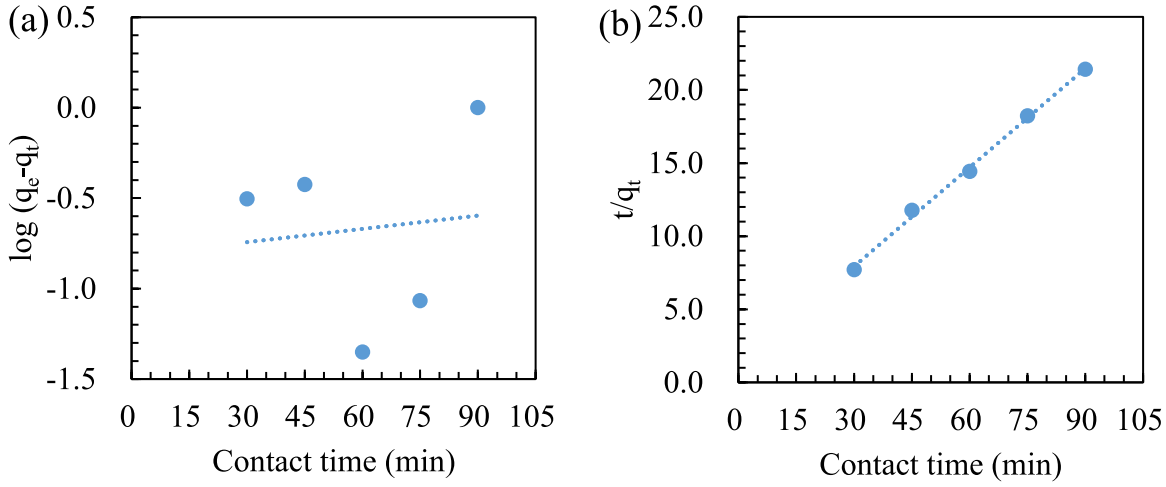

Fig. 10. Adsorption kinetics were analyzed using pseudo-first-order (a) and pseudo-second-order (b) curves.

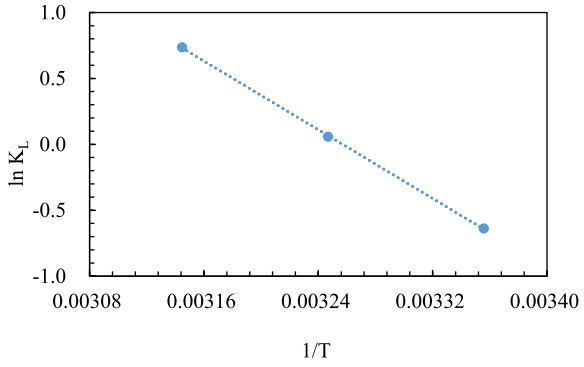

Fig. 12. Thermodynamic adsorption of AB1 onto SA/PAA/Fe.

Table 5
Thermodynamic parameters of AB1 adsorption onto SA/PAA/Fe.

Temp (K)	K	ΔG° (kJ.mol^{-1})	ΔH° (kJ.mol^{-1})	ΔS° (kJ.mol^{-1} K^{-1})	R^2
298	0.528	1.583	54.157	176.390	0.9999
308	1.060	-0.149			
318	2.088	-1.947			

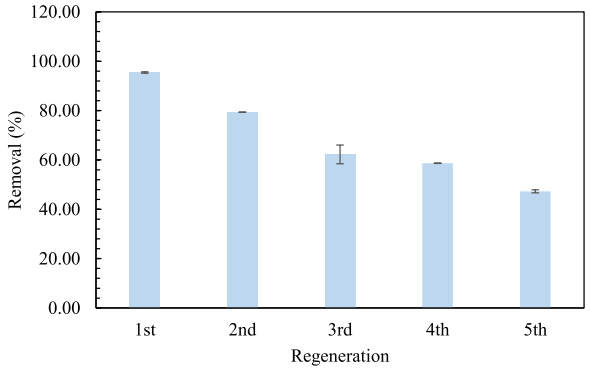

Fig. 13. Regeneration of SA/PAA-Fe for AB1 adsorption.

Table 6
Comparison of the adsorption capabilities related to anionic dye.

Adsorbents	Anionic dye	q_e (mg/g)	Reference
Gracilaria persica biomass	Acid black 1	9	[38]
Fly ash	Methyl orange	3.9	[39]
Fly ash	Reactive blue 171	3.75	[40]
Lignocellulosic waste biomass activated carbon	Acid black 1	3.8	[41]
Fly ash	Acid red 91	1.75	[42]
SA/PAA-Fe	Acid black 1	4.77	This study

4. Conclusion

This investigation revealed the exceptional efficacy of SA/PAA-Fe in eliminating AB1 from aqueous solution. Several factors such as dosage of adsorbent, pH, initial concentration, and temperature were identified as influential parameters for the sorption of AB1. The adsorption capacity of AB1 was 4.77 mg/g, and the removal percentage was 95.43 %. Langmuir and pseudo-second-order models were used on this study to obtain information on the isotherms and kinetics of the adsorption process. These findings suggest that the adsorption process is a monolayer and involves chemical adsorption. Thermodynamic analyses (ΔG°, ΔH°, and ΔS°) demonstrated that the adsorption process of AB1 was endothermic and spontaneous.

CRediT authorship contribution statement

Nur Maisarah Mohamad Sarbani: Writing – review & editing, Writing – original draft, Validation. **Endar Hidayat:** Writing – review & editing, Writing – original draft, Validation, Methodology, Investigation, Formal analysis, Data curation, Conceptualization. **Yoshiharu Mitoma:** Supervision. **Sadaki Samitsu:** Writing – review & editing, Validation, Supervision, Investigation. **Seiichiro Yonemura:** Supervision. **Mitsuru Aoyagi:** Supervision. **Hiroyuki Harada:** Supervision, Project administration, Funding acquisition.

Data availability

Data will be made available on request.

Declaration of Competing Interest

The authors declare that they have no known competing financial interests or personal relationships that could have appeared to influence the work reported in this paper.

Acknowledgement

Endar Hidayat (E.H.) wishes to express thank to the MEXT Scholarship for providing sponsorship during studies at the Prefectural University of Hiroshima. E. H. would like to express gratitude to the National Institute for Materials Science (NIMS), Japan, for accepting the research internship as well as to all the authors who have contributed to the completion of this study.

References

[1] Karimifard S, Alavi Moghaddam MR. Application of response surface methodology in physicochemical removal of dyes from wastewater: A critical review. Sci Total Environ 2018;640–641:772–97. https://doi.org/10.1016/j.scitotenv.2018.05.355.
[2] Wang P, Shen T, Li X, Tang Y, Li Y. Magnetic Mesoporous Calcium Carbonate-Based Nanocomposites for the Removal of Toxic Pb(II) and Cd(II) Ions from Water. ACS Appl Nano Mater 2020;3:1272–81. https://doi.org/10.1021/acsanm.9b02036.
[3] Wong S, Ghafar NA, Ngadi N, Razmi FA, Inuwa IM, Mat R, Amin NAS. Effective removal of anionic textile dyes using adsorbent synthesized from coffee waste. Sci Rep 2020;10. https://doi.org/10.1038/s41598-020-60021-6.
[4] Qurrat-ul-Ain Q-A, Khatoon J, Shah MR, Malik MI, Khan IAT, Khurshid S, Naz R. Convenient pH-responsive removal of Acid Black 1 by green < scp > l < /scp > -histidine/iron oxide magnetic nanoadsorbent from water: performance and mechanistic studies. RSC Adv 2019;9:2978–96. https://doi.org/10.1039/C8RA09279F.
[5] Piaskowski K, Świderska-Dąbrowska R, Zarzycki PK. Dye Removal from Water and Wastewater Using Various Physical, Chemical, and Biological Processes. J AOAC Int 2018;101:1371–84. https://doi.org/10.5740/jaoacint.18-0051.
[6] Liang C, Ren J, El Hankari S, Huo J. Aqueous Synthesis of a Mesoporous Zr-Based Coordination Polymer for Removal of Organic Dyes. ACS Omega 2020;5:603–9. https://doi.org/10.1021/acsomega.9b03192.
[7] Srivatsav P, Bhargav BS, Shanmugasundaram V, Arun J, Gopinath KP, Bhatnagar A. Biochar as an eco-friendly and economical adsorbent for the removal of colorants (Dyes) from aqueous environment: A review. Water (Switz) 2020;12. https://doi.org/10.3390/w12123561.
[8] Wiśniewska M, Nowicki P, Nosal-Wiercińska A, Pietrzak R, Szewczuk-Karpisz K, Ostolska I, Sternik D. Adsorption of poly(acrylic acid) on the surface of microporous activated carbon obtained from cherry stones. Colloids Surf A Physicochem Eng Asp 2017;514:137–45. https://doi.org/10.1016/j.colsurfa.2016.11.053.
[9] Au VKM. Recent Advances in the Use of Metal-Organic Frameworks for Dye Adsorption. Front Chem 2020;8. https://doi.org/10.3389/fchem.2020.00708.
[10] Torabinejad A, Nasirizadeh N, Yazdanshenas ME, Tayebi HA. Synthesis of conductive polymer-coated mesoporous MCM-41 for textile dye removal from aqueous media. J Nanostructure Chem 2017;7:217–29. https://doi.org/10.1007/s40097-017-0232-7.
[11] Liu Z, Pan L, Hu F, Hu Y. Advanced landfill leachate biochemical effluent treatment using Fe-Mn/AC activates O3/Na2S2O8 process: process optimization, wastewater quality analysis, and activator characterization. Environ Sci Pollut Res 2020;27:15337–49. https://doi.org/10.1007/s11356-020-08046-2.

[12] Zhao X. Multi-scale multi-mechanism design of tough hydrogels: building dissipation into stretchy networks. Soft Matter 2014;10:672–87. https://doi.org/10.1039/C3SM52272E.
[13] Chen Z, Zhao X, Yu Y, Zhou J. Structure and Properties of Cellulose Strengthened Poly(Acrylic Acid) Hydrogels. Macromol Mater Eng 2024. https://doi.org/10.1002/mame.202300454.
[14] Candry P, Godfrey BJ, Wang Z, Sabba F, Dieppa E, Fudge J, Balogun O, Wells G, Winkler MKH. Tailoring polyvinyl alcohol-sodium alginate (PVA-SA) hydrogel beads by controlling crosslinking pH and time. Sci Rep 2022;12. https://doi.org/10.1038/s41598-022-25111-7.
[15] Craciun G, Calina IC, Demeter M, Scarisoreanu A, Dumitru M, Manaila E. Poly (Acrylic Acid)-Sodium Alginate Superabsorbent Hydrogels Synthesized by Electron Beam Irradiation Part I: Impact of Initiator Concentration and Irradiation Dose on Structure, Network Parameters and Swelling Properties. Materials 2023;16. https://doi.org/10.3390/ma16134552.
[16] Thakur S, Arotiba OA. Synthesis, swelling and adsorption studies of a pH-responsive sodium alginate–poly(acrylic acid) superabsorbent hydrogel. Polym Bull 2018;75:4587–606. https://doi.org/10.1007/s00289-018-2287-0.
[17] Isawi H. Using Zeolite/Polyvinyl alcohol/sodium alginate nanocomposite beads for removal of some heavy metals from wastewater. Arab J Chem 2020;13:5691–716. https://doi.org/10.1016/j.arabjc.2020.04.009.
[18] Hu T, Liu Q, Gao T, Dong K, Wei G, Yao J. Facile Preparation of Tannic Acid-Poly (vinyl alcohol)/Sodium Alginate Hydrogel Beads for Methylene Blue Removal from Simulated Solution. ACS Omega 2018;3:7523–31. https://doi.org/10.1021/acsomega.8b00577.
[19] Chen T, Liu H, Gao J, Hu G, Zhao Y, Tang X, Han X. Efficient removal of methylene blue by bio-based sodium alginate/lignin composite hydrogel beads. Polym (Basel) 2022;14. https://doi.org/10.3390/polym14142917.
[20] Voo WP, Ooi CW, Islam A, Tey BT, Chan ES. Calcium alginate hydrogel beads with high stiffness and extended dissolution behaviour. Eur Polym J 2016;75:343–53. https://doi.org/10.1016/j.eurpolymj.2015.12.029.
[21] ALSamman MT, Sánchez J. Chitosan- and Alginate-Based Hydrogels for the Adsorption of Anionic and Cationic Dyes from Water. Polym (Basel) 2022;14:1498. https://doi.org/10.3390/polym14081498.
[22] Massana Roquero D, Othman A, Melman A, Katz E. Iron(iii)-cross-linked alginate hydrogels: A critical review. Mater Adv 2022;3:1849–73. https://doi.org/10.1039/d1ma00959a.
[23] Frent OD, Vicas LG, Duteanu N, Morgovan CM, Jurca T, Pallag A, Muresan ME, Filip SM, Lucaciu RL, Marian E. Sodium Alginate—Natural Microencapsulation Material of Polymeric Microparticles. Int J Mol Sci 2022;23. https://doi.org/10.3390/ijms232012108.
[24] Łętocha A, Miastkowska M, Sikora E. Preparation and Characteristics of Alginate Microparticles for Food, Pharmaceutical and Cosmetic Applications. Polym (Basel) 2022;14. https://doi.org/10.3390/polym14183834.
[25] Sing KSW. Reporting physisorption data for gas/solid systems with special reference to the determination of surface area and porosity (Recommendations 1984). Pure Appl Chem 1985;57:603–19. https://doi.org/10.1351/pac198557040603.
[26] Modrzejewska Z. Sorption mechanism of copper in chitosan hydrogel. React Funct Polym 2013;73:719–29. https://doi.org/10.1016/j.reactfunctpolym.2013.02.014.
[27] Patel A, Soni S, Mittal J, Mittal A, Arora C. Sequestration of crystal violet from aqueous solution using ash of black turmeric rhizome. Desalin Water Treat 2021;220:342–52. https://doi.org/10.5004/dwt.2021.26911.
[28] Qurrat-Ul-Ain, Khatoon J, Shah MR, Malik MI, Khan IAT, Khurshid S, Naz R. Convenient pH-responsive removal of Acid Black 1 by green l-histidine/iron oxide magnetic nanoadsorbent from water: Performance and mechanistic studies. RSC Adv 2019;9:2978–96. https://doi.org/10.1039/c8ra09279f.
[29] Naushad M, Ahamad T, Al-Maswari BM, Abdullah Alqadami A, Alshehri SM. Nickel ferrite bearing nitrogen-doped mesoporous carbon as efficient adsorbent for the removal of highly toxic metal ion from aqueous medium. Chem Eng J 2017;330:1351–60. https://doi.org/10.1016/j.cej.2017.08.079.
[30] Zeydouni G, Kianizadeh M, Omidi Khaniabadi Y, Nourmoradi H, Esmaeili S, Mohammadi MJ, Rashidi R. Eriochrme black-T removal from aqueous environment by surfactant modified clay: equilibrium, kinetic, isotherm, and thermodynamic studies. Toxin Rev 2019;38:307–17. https://doi.org/10.1080/15569543.2018.1455214.
[31] Hidayat E, Harada H, Mitoma Y, Yonemura S, Halem HIA. Rapid Removal of Acid Red 88 by Zeolite/Chitosan Hydrogel in Aqueous Solution. Polym (Basel) 2022;14. https://doi.org/10.3390/polym14050893.
[32] Hidayat E, Mohamad Sarbani NMB, Yonemura S, Mitoma Y, Harada H. Application of Box–Behnken Design to Optimize Phosphate Adsorption Conditions from Water onto Novel Adsorbent CS-ZL/ZrO/Fe3O4: Characterization, Equilibrium, Isotherm, Kinetic, and Desorption Studies. Int J Mol Sci 2023;24. https://doi.org/10.3390/ijms24119754.
[33] Lita AL, Hidayat E, Mohamad Sarbani NM, Harada H, Yonemura S, Mitoma Y, Herviyanti, Gusmini. Glyphosate Removal from Water Using Biochar Based Coffee Husk Loaded Fe3O4. Water (Basel) 2023;15:2945. https://doi.org/10.3390/w15162945.
[34] Mohamad Sarbani NM, Hidayat E, Naito K, Mitoma Y, Harada H. Cr (VI) and Pb (II) Removal Using Crosslinking Magnetite-Carboxymethyl Cellulose-Chitosan Hydrogel Beads. Gels 2023;9:612. https://doi.org/10.3390/gels9080612.
[35] Cordova Estrada AK, Cordova Lozano F, Lara Díaz RA. Thermodynamics and kinetic studies for the adsorption process of methyl orange by magnetic activated carbons. Air, Soil Water Res 2021;14. https://doi.org/10.1177/11786221211013336.
[36] Munagapati VS, Yarramuthi V, Kim Y, Lee KM, Kim DS. Removal of anionic dyes (Reactive Black 5 and Congo Red) from aqueous solutions using Banana Peel Powder as an adsorbent. Ecotoxicol Environ Saf 2018;148:601–7. https://doi.org/10.1016/j.ecoenv.2017.10.075.
[37] El-Sabbagh SM, Mira HI, Desouky OA, Hussien SS, Elgohary DM, Ali AO, El Naggar AMA. Synthesis of fungal chitosan–polystyrene modified by nanoparticles of binary metals for the removal of heavy metals from waste aqueous media. RSC Adv 2023;13:29735–48. https://doi.org/10.1039/D3RA04451C.
[38] Kousha M, Daneshvar E, Dopeikar H, Taghavi D, Bhatnagar A. Box–Behnken design optimization of Acid Black 1 dye biosorption by different brown macroalgae. Chem Eng J 2012;179:158–68. https://doi.org/10.1016/j.cej.2011.10.073.
[39] Potgieter JH, Pardesi C, Pearson S. A kinetic and thermodynamic investigation into the removal of methyl orange from wastewater utilizing fly ash in different process configurations. Environ Geochem Health 2021;43:2539–50. https://doi.org/10.1007/s10653-020-00567-6.
[40] Banerjee S, Sharma GC, Chattopadhyaya MC, Sharma YC. Kinetic and equilibrium modeling for the adsorptive removal of methylene blue from aqueous solutions on of activated fly ash (AFSH). J Environ Chem Eng 2014;2:1870–80. https://doi.org/10.1016/j.jece.2014.06.020.
[41] Nethaji S, Sivasamy A. Adsorptive removal of an acid dye by lignocellulosic waste biomass activated carbon: Equilibrium and kinetic studies. Chemosphere 2011;82:1367–72. https://doi.org/10.1016/j.chemosphere.2010.11.080.
[42] Ramakrishna KR, Viraraghavan T. Dye removal using low cost adsorbents. Water Sci Technol 1997;36. https://doi.org/10.1016/S0273-1223(97)00387-9.